LCM汚染マウス血清のIFA

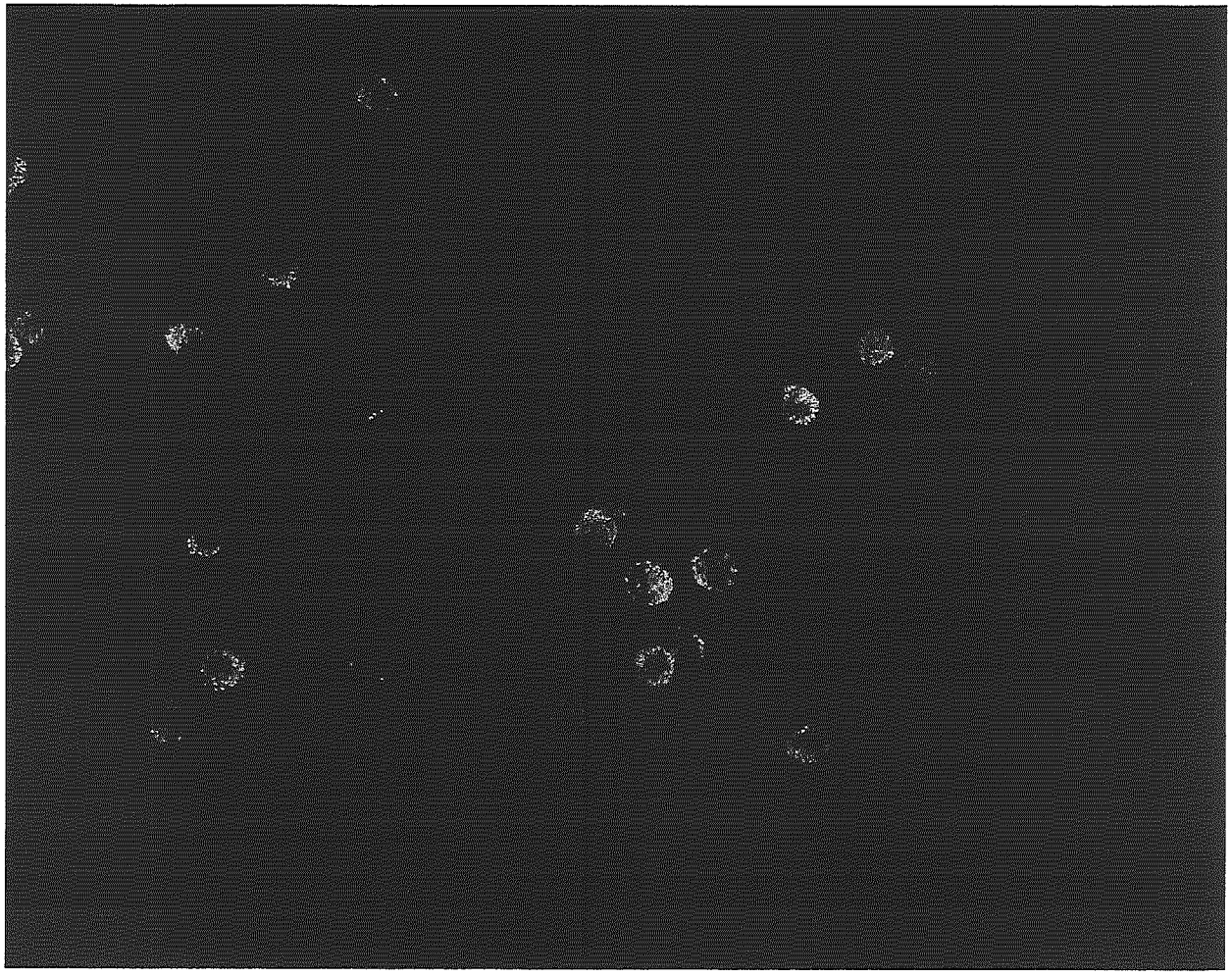

研究成果の刊行に関する一覧表

書籍

著者氏名	論文タイトル名	書籍全体の編集者名	書籍名	出版社名	出版地	出版年	ページ
Rockwood,S.F., Fray.M.D. and Nakagata, N.	Managing Success:Mutant Mouse Repositories	John P. Sunderberg Tsutomu Ichiki	Genetically Engineered Mice Handbook.	Taylor and Francis	Florida USA	2005	27-38
Fray.M.D., Glenister.P.H., Rockwood,S.F., Kaneko,T.and Nakagata,N.	Biological Methods for Archiving and Maintaining Mutant Laboratory Mice.	John P. Sunderberg Tsutomu Ichiki	Genetically Engineered Mice Handbook,	Taylor and Francis	Florida USA	2005	83-112
Ogura A, Inoue K, Ogonuki N, and Miki H	The present status of somatic cell cloning.	Sundberg JP and Ichiki T	Genetically Engineered Mice	CRC Press	Boca Raton, USA	2005	125-130
井上貴美子、小倉淳郎	核移植とリプログラミング	仲野 徹	再生医療のための分子生物学	コロナ社	東京	2006	66-79
蓮輪英毅，岡部勝	RNAiによる哺乳動物個体レベルでのノックダウン	中村 義一，大内 将司	RNA工学の最前線	シーエムシー出版	東京	2005	67-76
Katoh H	Genetic monitoring of mice	Sundberg JP, Ichiki T	Handbooko on genetically engineered mice	CRC Press	USA	2005	143-156

雑誌

発表者氏名	論文タイトル名	発表誌名	巻号	ページ	出版年
Cho A-R, Uchio-Yamada K, Torigai T, Miyamoto T, Miyoshi I, Matsuda J, Kurosawa T, Kon Y, Asano A, Sasaki N,Aguil T.	Deficiency of the tensin2 gene in the ICGN mouse, an animal model for congenital nephrotic syndrome.	Mammalian Genome (in press)			2006
Okada T, Ishii Y, Masujin K, Yasoshima A, Matsuda J, Ogura A, Nakayama H, Kunieda T, Doi K.	The critical roles of serum/glucocorticoid regulated kinase 3 (SGK3) in the hair follicle morphogenesis and homeostasis: the allelic difference provides novel insights into hair follicle biology.	American Journal of Pathology (in press)			2006
Noguchi Y, Takano K, Koura M, Uchio-Yamada K,	Sequence analysis of cDNA encoding rabbit follicle-stimulating hormone beta-subunit precursor	Gen. Comp. Endocrinol (in press)			2006

Matsuda J, Suzuki O.	protein.				
Hasegawa H, Sawa H, Lewis M, Orba Y, Sheehy N, Yamamoto Y, Ichinohe T, Tsunetsugu-Yokota Y, Katano H, Takahashi H, Matsuda J, Sata T, Kurata T, Nagashima K, Hall WW.	Development of Thymus-Derived T-cell Leukemia/Lymphoma in Mice Transgenic for the Tax gene of Human T-Lymphotropic Virus Type-I (HTLV-I).	Nature Medicine (in press)			2006
Sekita Y, Wagatsuma H, Irie M, Kobayashi S, Kohda K, Matsuda J, Yokoyama M, Ogura A, Schuster-Gossler K, Gossler A, Ishino F, Kaneko-Ishino T.	Aberrant regulation of imprinted gene expression in *Gtl2*^{lacZ} mice.	Cytogenet Genome Res (in press)			2006
Suzuki O, Hata T, Takekawa N, Koura M, Takano K, Yamamoto Y, Noguchi Y, Uchio-Yamada K, Matsuda J.	Transgene insertion pattern analysis using genomic walking in a transgenic mouse line.	Exp Anim	55(1)	65-69	2006
Mochida K, Wakayama T, Takano, Noguchi Y, Yamamoto Y, Suzuki O, Matsuda J, Ogura A.	Birth of Offspring after Transfer of Mongolian Gerbil (*Meriones unguiculatus*) Embryos Cryopreserved by Vitrification.	Mol Reprod Dev	70	464-70	2005
Valdez D.M., Miyamoto A., Hara T., Edashige K., Kasai M.	Sensitivity to chilling of medaka (*Oryzias latipes*) embryos at various developmental stages.	Theriogenology	64(1)	112-122	2005
Valdez D.M., Miyamoto A., Hara T., Seki S., Kasai M., Edashige K.	Water- and cryoprotectant-permeability of mature and immature oocytes in the medaka (*Oryzias latipes*).	Cryobiology	50(1)	93-102	2005
Pedro P.B., Yokoyama E., Zhu S.E., Yoshida N., Valdez D.M., Tanaka M., Edashige E., Kasai M.	Permeability of mouse oocytes and embryos at various developmental stages to five cryoprotectants.	Journal of Reproduction and Development	51(1)	235-246	2005
Edashige K., Tanaka M., Ichimaru N., Ota S., Yazawa K., Higashino Y., Sakamoto M., Yamaji Y., Kuwano T., Valdez D.M., Kleinhans F.W., Kasai M.	Channel-dependent permeation of water and glycerol in mouse morulae.	Biology of Reproduction (in press)			

Kaneko, T., Nakagata, N.	Relation between storage temperature and fertilizing ability of freeze-dried mouse spermatozoa.	Comp Med.	55	140-144	2005
Sakamoto, W., Kaneko, T., Nakagata, N.	Use of frozen-thawed oocytes for Efficient production of normal offspring from cryopreserved mouse spermatozoa showing low fertility.	Comp Med.	55	136-139	2005
Yoshimoto, N,. Shimoda, K, Mori, Y., Honda, R., Okamura, H,. Ide, Y., Nakashima, T.,Nakagata, N., Torii, R., Yoshikawa, Y., Hayasaka, I.	Ovarian follicular development stimulated by leuprorelin acetate plus human menopausal gonadotropin in chimpanzees.	J Med Primatol.	34	73-85	2005
Taniwaki, T., Haruna, K., Nakamura, H., Sekimoto, T., Oike, Y., Imaizumi, T., Saito, F., Muta, M., Soejima, Y., Utoh, A., Nakagata, N., Araki, M., Yamamura, K., Araki, K.	Characterization of an exchangeable gene trap using pU-17 carrying a stop codon-beta geo cassette.	Dev Growth Differ	47	163-172	2005
Oike, Y., Akao, M., Yasunaga, K., Yamauchi, T., Morisada, T., Ito, Y., Urano, T., Kimura,Y., Kubota, Y., Maekawa, H., Miyamoto, T., Miyata, K., Matsumoto, S., Sakai, J., Nakagata,N. Takeya, M., Koseki, H., Ogawa, Y., Kadowaki, T., Suda,T.	Angiopoietin-related growth factor antagonizes obesity and insulin resistance.	Nat Med.	11	400-408	2005
Okazuka K, Wakabayashi Y, Kashihara M, Inoue J, Sato T, Yokoyama M, Aizawa S, Aizawa Y, Mishima Y, Kominami R	p53 prevents maturation of T cell development to the immature CD4-CD8+ stage in Bcl11b-/- mice.	Biochem Biophys Res Commun	328	545-549	2005
Shiura H, Miyoshi N, Konishi A, Wakisaka-Saito N, Suzuki R, Muguruma K, Kohda T, Wakana S, Yokoyama M, Ishino F, Kaneko-Ishino T	Meg1/Grb10 overexpression causes postnatal growth retardation and insulin resistance via negative modulation of the IGF1R and IR cascades.	Biochem Biophys Res Commun	329	909-916	2005

Ono R, Nakamura K, Inoue K, Naruse M, Usami T, Wakisaka-Saito N, Hino T, Suzuki-Migishima R, Ogonuki N, Miki H, Ogura A, Yokoyama M, Kaneko-Ishino T, Ishino F	Deletion of Peg10, animprinted gene acquired from a retrotransposon, causes early embryonic lethality.	Nat Genet	38	101-106	2006
Kwon J., Mochida K., Wang Y.L., Sekiguchi S., Sankai T., Aoki S., Ogura A., Yoshikawa Y., Wada K.	Ubiquitin C-terminal hydrolase L-1 is essential for the early apoptotic wave of germinal cells and for sperm quality control during Spermatogenesis.	Biol. Reprod.	73	29-35	2005
Tanemura K., Ogura A., Cheong C., Gotoh H., Matsumoto K., Sato E., Hayashi Y., Lee H.W., Kondo T.	Dynamic rearrangement of telomeres during spermatogenesis in mice.	Dev. Biol.	28	196-207	2005
Kanatsu-Shinohara M., Miki H., Inoue K., Ogonuki N., Toyokuni S., Ogura A., Shinohara T.	Germline niche transplantation restores fertility in infertile mice.	Hum. Reprod.	20	2376-2382	2005
Inoue K., Wakao H., Ogonuki N., Miki H., Seino K., Nambu-Wakao R., Noda S., Miyoshi H., Koseki H., Taniguchi M., Ogura A.	Generation of cloned mice by direct nuclear transfer from natural killer T cells.	Curr. Biol.	15	1114-1118	2005
Ogura A., Ogonuki N., Miki H., Inoue K.	Microinsemination and nuclear transfer using male germ cells.	Int. Rev. Cytol.	246	189-229	2005
Ogonuki N., Inoue K., Miki H., Mochida K., Hatori M., Okada H., Takeiri S., Shimozawa N., Nagashima H., Sankai T., Ogura A.	Differential development of rabbit embryos following microinsemination with sperm and spermatids.	Mol. Reprod. Dev.	72	411-417	2005
Kanatsu-Shinohara M., Ogonuki N., Iwano T., Lee J., Kazuki Y., Inoue K., Miki H., Takehashi M., Toyokuni S., Shinkai Y., Oshimura M., Ishino F., Ogura A., Shinohara T.	Genetic and epigenetic properties of mouse male germline stem cells during long-term culture.	Development	132	4155-4163	2005
Yamagata K., Yamazaki T., Yamashita M., Hara Y., Ogonuki N., Ogura A.	Noninvasive visualization of molecular events in the mammalian zygote.	Genesis	43	71-79	2005
Kohda T., Inoue K.,	Variation in gene expression and	Biol. Reprod.	73	1302-131	2005

Ogonuki N., Miki H., Naruse M., Kaneko-Ishino T., Ogura A., Ishino F.	aberrantly regulated 1 chromosome regions in cloned mice.			1	
Kanatsu-Shinohara M., Inoue K., Lee J., Miki H., Ogonuki N., Toyokuni S., Ogura A., Shinohara T.	Anchorage-independent growth of mouse male germline stem cells in vitro.	Biol. Reprod.	74	522-529	2006
Kanatsu Shinohara, M., Miki, H., Inoue, K., Ogonuki, N., Toyokuni, S., Ogura, A., and Shinohara, T	Long-term culture of mouse male germline stem cells under serum- or feeder-free conditions	Biol. Reprod.	72	985-991	2005
Miki H., Ogonuki N., Inoue K., Baba T., Ogura A.	Improvement of cumulus-free oocyte maturation in vitro and its application to microinsemination with primary spermatocytes in mice.	J. Reprod. Dev. (in press)			2006
Inoue K., Ogonuki N., Miki H., Hirose M., Noda S., Kim J. M., Aoki F., Miyoshi H., Ogura A.	Inefficient reprogramming of the hematopoietic stem cell genome following nuclear transfer.	J. Cell Sci. (in press)			2006
S. Kobayashi, A. Isotani, N. Mise, M. Yamamoto, Y. Fujihara, K. Kaseda, T. Nakanishi, M. Ikawa, H. Hamada, K. Abe and M. Okabe	Comparison of gene expression in male and female mouse blastocysts revealed imprinting of the x-linked gene, rhox5/pem, at preimplantation stages.	Curr Biol	16(2)	166-72	2006
G. Kondoh, H. Tojo, Y. Nakatani, N. Komazawa, C. Murata, K. Yamagata, Y. Maeda, T. Kinoshita, M. Okabe, R. Taguchi and J. Takeda	Angiotensin-converting enzyme is a GPI-anchored protein releasing factor crucial for fertilization.	Nat Med	11(2)	160-166	2005
N. Inoue, M. Ikawa, A. Isotani and M. Okabe	The immunoglobulin superfamily protein Izumo is required for sperm to fuse with eggs.	Nature	434(7030)	234-8	2005
A. Isotani, T. Nakanishi, S. Kobayashi, J. Lee, S. Chuma, N. Nakatsuji, F. Ishino and M. Okabe	Genomic imprinting of XX spermatogonia and XX oocytes recovered from XX{leftrightarrow}XY chimeric testes	Proc Natl Acad Sci U S A	102(11)	4039-44	2005
K. Yahata, H. Kishine, T. Sone, Y. Sasaki, J. Hotta, J. D. Chesnut, M. Okabe and F.	Multi-gene Gateway clone design for expression of multiple heterologous genes in living cells: Conditional gene expression at near	J Biotechnol	118(2)	123-34	2005

Imamoto	physiological levels				
H. Tanaka, N. Iguchi, A. Isotani, K. Kitamura, Y. Toyama, Y. Matsuoka, M. Onishi, K. Masai, M. Maekawa, K. Toshimori, M. Okabe and Y. Nishimune	HANP1/H1T2, a Novel Histone H1-Like Protein Involved in Nuclear Formation and Sperm Fertility.	Mol Cell Biol	25(16)	7107-19	2005
X. Wang, S. Inoue, J. Gu, E. Miyoshi, K. Noda, W. Li, Y. Mizuno-Horikawa, M. Nakano, M. Asahi, M. Takahashi, N. Uozumi, S. Ihara, S. H. Lee, Y. Ikeda, Y. Yamaguchi, Y. Aze, Y. Tomiyama, J. Fujii, K. Suzuki, A. Kondo, S. D. Shapiro, C. Lopez-Otin, T. Kuwaki, M. Okabe, K. Honke and N. Taniguchi	Dysregulation of TGF-beta1 receptor activation leads to abnormal lung development and emphysema-like phenotype in core fucose-deficient mice.	Proc Natl Acad Sci U S A	102(44)	15791-6	2005
岡部勝	遺伝子操作動物を通して見る受精のメカニズム	関西実験動物研究会会報	26	74-7	2005
井上直和，岡部勝	受精の膜融合必須分子 Izumo の発見	細胞工学	24(5)	490-1	2005
Takabayashi, S. and Katoh, H.	A mutant mouse with severe anemia and skin abnormalities controlled by a new allele of the flaky skin (fsn) locus.	Exp. Anim	54	339-347	2005
Katoh, H., Yoshino, S., Inui, Y., Honda, S. and Takabayashi, S.	Microsatellite genotyping for genetic quality testing using sperm cells in the mouse.	Exp. Anim	54	373-376	2005

Exp. Anim. 55(1), 65–69, 2006

—Note—

Transgene Insertion Pattern Analysis Using Genomic Walking in a Transgenic Mouse Line

Osamu SUZUKI*, Tomoko HATA, Naho TAKEKAWA, Minako KOURA*, Kaoru TAKANO*, Yoshie YAMAMOTO, Yoko NOGUCHI*, Kozue UCHIO-YAMADA*, and Junichiro MATSUDA*

Department of Veterinary Science, National Institute of Infectious Diseases, 1–23–1 Toyama, Shinjuku-ku, Tokyo 162-8640, Japan
**Current address: Laboratory of Experimental Animal Models, National Institute of Biomedical Innovation, 7–6–8 Saitoasagi, Ibaraki-shi, Osaka 567-0085, Japan*

Abstract: *A transgene mapping technique (Noguchi* et al., *Exp. Anim. 53:103-111, 2004) is described that can be used to analyze transgene integration patterns in transgenic mice. The technique was used to reveal that a transgenic mouse line (GM1-sy#116) harbored inverted and direct tandem repeats of both intact and partial pCAGGS-based transgenes in the G2 region of chromosome 1. This complicated concatenation of transgenes may have been caused by simple end-joining of DNA constructs fragmented by exposure to UV transillumination during gel-purification, and by nuclease digestion inside zygote pronuclei. The results suggest that care should be taken to avoid unwanted fragmentation during the preparation of vector constructs.*

Key words: *genomic walking, integration pattern, transgene*

Simple and accurate genotyping methods, especially those designed to assess zygosity, are necessary for the efficient use and management of transgenic laboratory animals. In a previous report, we described a simple and efficient method for genetic mapping and zygosity analysis of transgenes [12]. Sequences flanking the trangenes are determined using genomic walking, which allows the transgene insertion sites in chromosomes to be located by searching a genome database. In addition, flanking primers can be designed to assess the zygosity of the transgene loci in transgenic animals using PCR [10]. Here, we report that the genomic walking technique can be used to determine the transgene insertion pattern, as well as the flanking sequences, and we discuss the mechanism of transgene integration into chromosomes.

We used a transgenic mouse line, GM1-sy#116, with a C57BL/6JJmsSlc background, which was produced in our laboratory by zygote microinjection of transgene constructs based on a pCAGGS plasmid [11]. The constructs (Fig. 1A) consisted of fragments generated from the *Sal*I–*Hin*dIII site of plasmid pCAGGS, which contains a ganglioside GM1 synthase cDNA [5] cloned in our laboratory from C57BL/6J genomic DNA. All ani-

(Received 4 July 2005 / Accepted 26 September 2005)
Address corresponding: O. Suzuki, Laboratory of Experimental Animal Models, National Institute of Biomedical Innovation, 7–6–8 Saitoasagi, Ibaraki-shi, Osaka 567-0085, Japan

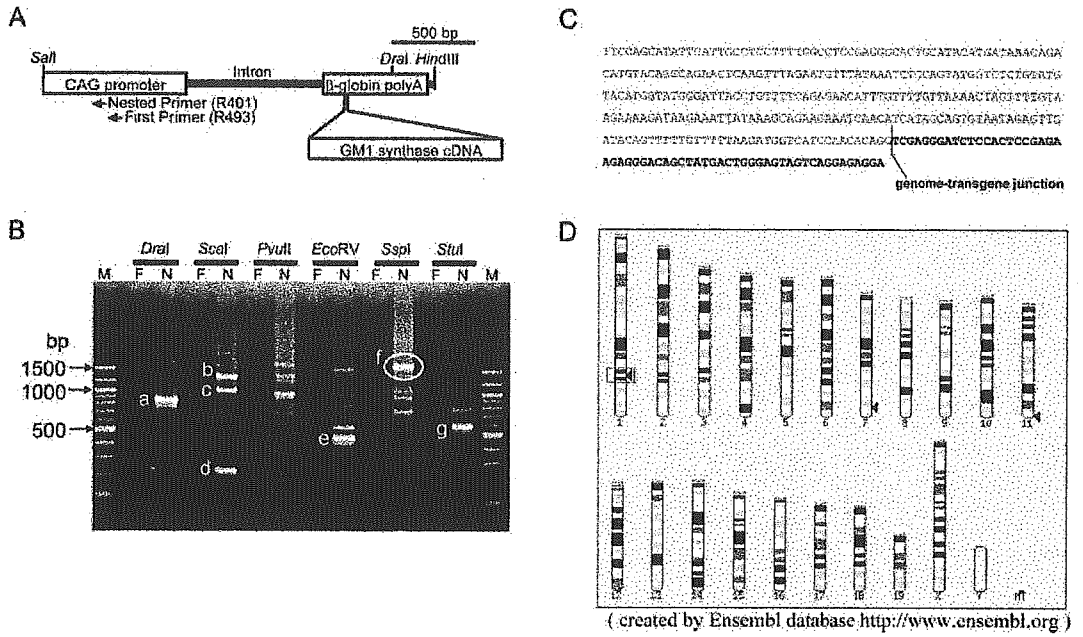

Fig. 1. Chromosomal mapping in the transgenic mouse line GM1sy#116. The integrated transgene construct contained GM1 synthase cDNA (A). The products of first (F) and nested (N) PCR amplifications using GM1sy#116 genomic libraries were separated by agarose gel electrophoresis (B). The sequence (C) flanking the transgene was determined using an approximately 1.5-kb band amplified from an *SspI* library (band f in B). Other bands (a-e and g) did not provide flanking sequence information. A search of the Ensembl genome database using the flanking sequence, under the condition *Expectation value* < 0.001, located the transgene to the G2 region of chromosome 1 (boxed in D). M, 100-bp DNA ladder.

mal experiments were performed according to the Guides for Animal Experiments Performed at the NIID.

The sequences around the transgenes were determined by genomic walking using the method described previously [12], but with different transgene-specific primers, R493 (CCG CCC CCA TCG CTG CAC AAA ATA AT) and R401 (GTG GGG CTC ACC TCG ACC CAT GGT AAT). Some of the PCR amplicons (bands a–g in Fig. 1B) were gel-purified and sequenced directly using a DYEnamic ET Terminator Cycle Sequencing Kit (Amersham Biosciences, Piscataway, NJ, USA) with a DNA sequencer (RISA384, Shimadzu Biotech, Kyoto, Japan). The transgene insertion sites in the chromosomes were determined by BLAST search in the Ensembl genome database [9] of the sequences flanking the transgene (Fig. 1C). Searches were conducted over the Internet (http://www.ensembl.org), and were based on the mouse genome assembly NCBI build m33 (Fig. 1D).

Sequences of both transgene-genomic junctions were confirmed by PCR analyses using the flanking primer method. Two flanking primers, designated S412 (CAT GGT ATG GGA TTA CCT GTT TTC AGA) and R677 (CCC GGG CCC CAC ACT CAG AAC CTC TCT; Fig. 2A), were designed with the Primer3 program [15], using the flanking sequence around the transgene retrieved from the Ensembl database. A primer for the 3'-tail of the construct was also designed (pCAG-S2238; CCC TCT TCT CTT ATG AAG ATC CCT CGA CCT). PCR product formation was checked by PCR with tail DNA from transgenic mice and three combinations of primers (Fig. 2B): pCAG-S2238 only; pCAG-S2238 and S412; and pCAGGS-S2238 and R677. The zygosities of homozygous transgenic, hemizygous transgenic, and non-transgenic animals were determined by PCR of their tail DNA, the flanking primers, and pCAG-S2238 (Fig. 2C). Both PCR analyses were done under the following thermal conditions: 95°C for 15 min, followed by 30 cycles of 94°C for 5 s, 60°C for 5 s, and 72°C for 30 s. All PCR amplifications, including the genomic walking analysis, were conducted using a hot-start DNA

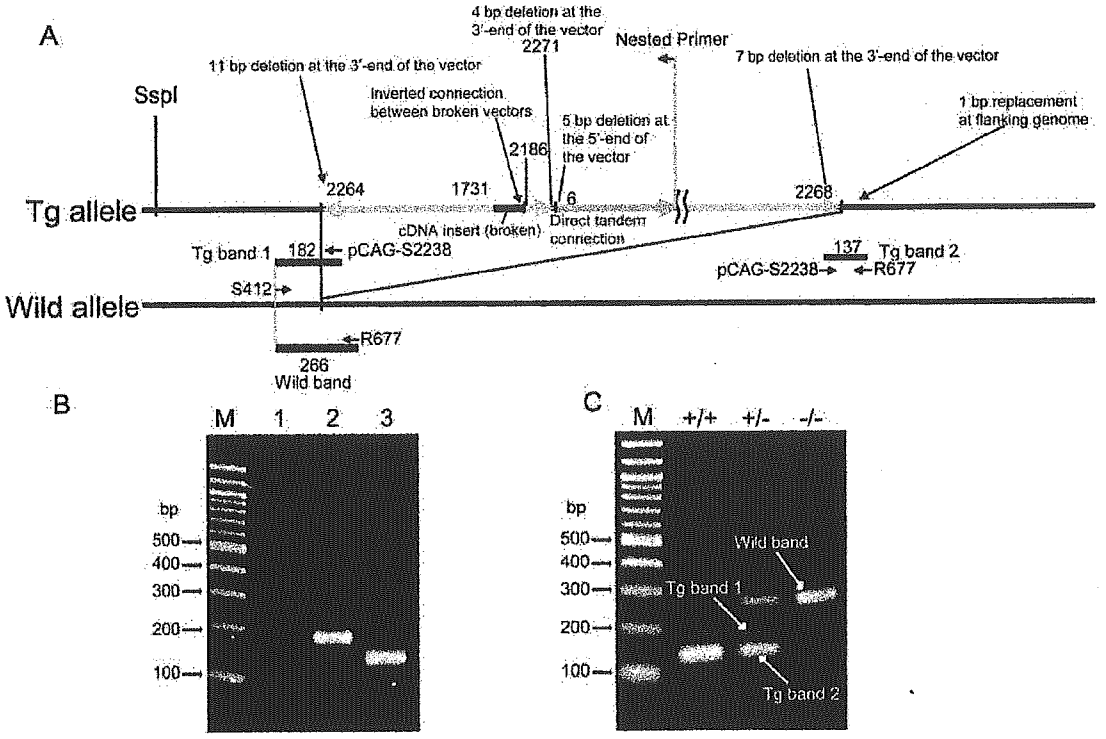

Fig. 2. Genomic configuration of GM1-sy#116, and the use of PCR to assess zygosity (A). The configuration of the transgene insert in the transgenic allele (Tg) and its corresponding wild-type allele (wild) are shown. One end of the insert was determined by genomic walking, and the other end by PCR with flanking primers. The directions of arrows over the inserts represent the 5'- to 3'-orientations of the vector constructs (arrowhead = 3'-end). Numbers along the inserts indicate the positions in pCAGGS. Approximately 10-bp deletions at each junction were detected, as shown in the figure. The positions of the three primers (S412, R677, and pCAG-S2238) used in a PCR experiment to determine zygosity, and the sizes of expected PCR products are also indicated. (B) Pre-evaluation of the PCR experiment. The primers were: lane 1, pCAG-S2238 only; lane 2, S412 and pCAG-S2238; lane 3, R677 and pCAG-S2238. M, 100-bp DNA ladder. (C) Determination of zygosity using PCR with the three primers, and genomic DNA from homozygous transgenic (+/+), hemizygous transgenic (+/–), and non-transgenic (–/–) mice. M, 100-bp DNA ladder.

polymerase (HotStarTaq; Qiagen, Hilden, Germany) in a Hybaid PCR Express Thermal Cycler (Thermo Hybaid, Ashford, Middlesex, UK). PCR products were separated by electrophoresis on a 2% agarose gel in Tris-acetate-EDTA buffer, and bands were detected by ethidium bromide staining and ultraviolet illumination (Figs. 1B, 2B and 2C).

Our method allowed the overall configuration of both ends of the transgene insert to be determined (Fig. 2A). One of the PCR bands (band f in Fig. 1B), which was approximately 1.5 kbp in length, contained about 500 bp of genome sequence flanking the transgene (Fig. 1C). A BLAST search of the sequence in the Ensembl database indicated that the transgene was inserted in the G2 region of chromosome 1 (Fig. 1D). The presence of an *Ssp*I restriction site in the genome sequence flanking the transgene was confirmed by the sequence around the transgene, which was retrieved from the database (data not shown). The full sequence of band f indicates the complicated insertion of constructs in the genome: one side of the genome faced the 3'-tail of a vector construct, and the construct was truncated at the middle of the inserted cDNA. Next to the truncated construct, direct repeats of the transgenes containing a short fragment of the 3'-tail of the construct were inversely concatenated and stretched at least to the position where the nested transgene-specific primer annealed. The structure of the other genome-transgene junction was revealed by PCR using three sets of flanking primers (Fig. 2B). No amplicons were produced by

PCR with pCAG-S2238 only (Fig. 2B-1), indicating the absence of tail-to-tail junction of transgenes as well as no formation of non-specific products by pCAG-S2238. The second set of primers (S412 and pCAG-S2238) confirmed one genome-transgene junction and showed a 182-bp band, as expected (Fig. 2B-2). The third set of primers (R677 and pCAG-S2238) showed a band of approximately 140 bp (Fig. 2B-3), which came from the other genome-transgene junctions. Direct sequencing confirmed that the band, which turned out to be 137 bp in length, was derived from the junction. Therefore, the 3'-tails of the transgenes were connected at both genome-transgene junctions. Although the full internal structure of the insert could not be identified by genomic walking, this is an example of irregular head-to-head type transgene-transgene junction, as described previously [12]. The zygosity was accurately determined using all three primers (Fig. 2C).

The mechanism of transgenesis is not fully understood, even though many kinds of transgenic animals have been produced (reviewed by e.g., [2]). Nevertheless, transgenesis seems to be accomplished in two steps: extrachromosomal concatenation of vector constructs, followed by integration into chromosomes [3]. Broad variation has been found at transgene-transgene and transgene-genome junctions in concatemers, such as deletions [7, 14], duplications [16], translocations of chromosomal DNA at the integration site [6, 13], and even insertions of sequences of unknown origin [16]. In our study, both types of junctions had approximately 10-base deletions, which may have been caused by so-called end-nibbling [14]. As Hamada *et al.* [7] discussed, the presence of nibbling at each junction suggests that linear concatemers were preferentially involved in the integration of the transgene into genomic DNA. Bishop [3] proposed a model in which concatemers are created by homologous recombination of circularly permuted linear molecules, which may explain the preferential formation of direct, rather than inverted, tandem repeats. In our case, however, it is more likely that concatemers of mixed orientation were formed by a simple random end-joining of DNA constructs, some of which had been fragmented before concatenation. While the fragmentation of DNA constructs can occur enzymatically inside zygote pronuclei, we suspect that the exposure to UV transillumination during gel-purification of our vector constructs was the most probable cause, because it has been shown that even a short period of transillumination induces serious DNA damage and profoundly reduces transformation frequencies [8]. Our results suggest that care should be taken to avoid unwanted fragmentation during the preparation of vector constructs.

Our results indicate that Bishop's model should be re-evaluated using a wide collection of transgenic patterns because of discrepancies with the fit of this model. In addition to events at transgene integration, attention should be paid to the possible involvement of the effect of transgene integration patterns on embryonic viability and modifications that occur after transgene integration, which are not accounted for by Bishop's model. If concatemer orientation affects embryonic viability, an embryo with direct (head-to-tail) tandem repeats of the transgene may be more viable than an embryo with inverted (head-to-head, tail-to-tail) tandem repeats. It is possible that inverted repeats that are integrated into the embryonic chromosome may be removed by palindrome deletion mechanisms [1]; if so, genomes of non-transgenic organisms may have transgene remnants (small fragments). Although difficult ($\leq$ 20% of transformed embryos reach birth [4]), further analysis of transgenic organisms would test the validity of this hypothesis.

Our results demonstrate the usefulness of the genomic walking technique to determine both the structure of transgenes and their flanking sequences. Together with gene expression assays, this technique should provide a powerful tool for revealing relationships between insertion pattern and expression efficiency of transgenes.

References

1. Akgun, E., Zahn, J., Baumes, S., Brown, G., Liang, F., Romanienko, P.J., Lewis, S., and Jasin, M. 1997. *Mol. Cell. Biol.* 17: 5559–5570.
2. Auerbach, A.B. 2004. *Acta Biochim. Pol.* 51: 9–31.
3. Bishop, J.O. 1996. *Reprod. Nutr. Dev.* 36: 607–618.
4. Brinster, R.L., Chen, H.Y., Trumbauer, M.E., Yagle, M.K., and Palmiter, R.D. 1985. *Proc. Natl. Acad. Sci. USA* 82: 4438–4442.
5. Daniotti, J.L., Martina, J.A., Zurita, A.R., and Maccioni, H.J. 1999. *J. Neurosci. Res.* 58: 318–327.
6. Gordon, J.W. and Ruddle, F.H. 1985. *Gene* 33: 121–136.
7. Hamada, T., Sasaki, H., Seki, R., and Sakaki, Y. 1993. *Gene* 128: 197–202.
8. Hartman, P.S. 1991. *Biotechniques* 11: 747–748.
9. Hubbard, T., Barker, D., Birney, E., Cameron, G., Chen,

Y., Clark, L., Cox, T., Cuff, J., Curwen, V., Down, T., Durbin, R., Eyras, E., Gilbert, J., Hammond, M., Huminiecki, L., Kasprzyk, A., Lehvaslaiho, H., Lijnzaad, P., Melsopp, C., Mongin, E., Pettett, R., Pocock, M., Potter, S., Rust, A., Schmidt, E., Searle, S., Slater, G., Smith, J., Spooner, W., Stabenau, A., Stalker, J., Stupka, E., Ureta-Vidal, A., Vastrik, I., and Clamp, M. 2002. *Nucleic Acids Res.* 30: 38–41.

10. Nagy, A., Gertsenstein, M., Vintersten, K., and Behringer, R. 2003. pp. 507–540. *In: Manipulating the Mouse Embryo*, Cold Spring Harbor Laboratory Press, New York.
11. Niwa, H., Yamamura, K., and Miyazaki, J. 1991. *Gene* 108: 193–199.
12. Noguchi, A., Takekawa, N., Einarsdottir, T., Koura, M., Noguchi, Y., Takano, K., Yamamoto, Y., Matsuda, J., and Suzuki, O. 2004. *Exp. Anim.* 53: 103–111.
13. Overbeek, P.A., Lai, S.P., Van Quill, K.R., and Westphal, H. 1986. *Science* 231: 1574–1577.
14. Rohan, R.M., King, D., and Frels, W.I. 1990. *Nucleic Acids Res.* 18: 6089–6095.
15. Rozen, S. and Skaletsky, H.J., *Primer3. Code available at http://www-genome.wi.mit.edu/genome_software/other/primer3.html.* 1998.
16. Wilkie, T.M. and Palmiter, R.D. 1987. *Mol. Cell. Biol.* 7: 1646–1655.

nature medicine

Thymus-derived leukemia-lymphoma in mice transgenic for the Tax gene of human T-lymphotropic virus type I

Hideki Hasegawa[1,2,8], Hirofumi Sawa[3,4,8], Martha J Lewis[2,5], Yasuko Orba[3], Noreen Sheehy[2], Yoshie Yamamoto[6], Takeshi Ichinohe[1], Yasuko Tsunetsugu-Yokota[7], Harutaka Katano[1], Hidehiro Takahashi[1], Junichiro Matsuda[6], Tetsutaro Sata[1], Takeshi Kurata[1], Kazuo Nagashima[3] & William W Hall[2]

Adult T-cell leukemia-lymphoma (ATLL) is a group of T-cell malignancies caused by infection with human T-lymphotropic virus type I (HTLV-I). Although the pathogenesis of ATLL remains incompletely understood, the viral regulatory protein Tax is centrally involved in cellular transformation. Here we describe the generation of HTLV-I Tax transgenic mice using the Lck proximal promoter to restrict transgene expression to developing thymocytes. After prolonged latency periods, transgenic mice developed diffuse large-cell lymphomas and leukemia with clinical, pathological and immunological features characteristic of acute ATLL. Transgenic mice were functionally immunocompromised and they developed opportunistic infections. Fulminant disease also developed rapidly in SCID mice after engraftment of lymphomatous cells from transgenic mice. Flow cytometry showed that the cells were $CD4^-$ and $CD8^-$, but $CD44^+$, $CD25^+$ and cytoplasmic $CD3^+$. This phenotype is indicative of a thymus-derived pre–T-cell phenotype, and disease development was associated with the constitutive activation of NF-κB. Our model accurately reproduces human disease and will provide a tool for analysis of the molecular events in transformation and for the development of new therapeutics.

HTLV-I infection is endemic in a number of well-defined geographical regions and it is estimated that as many as 20 million individuals are infected worldwide[1]. Although the vast majority of infected individuals remain clinically asymptomatic, some 2–5% will develop ATLL, which is a group of mature T-cell malignancies with distinct clinical presentations[2]. ATLL generally occurs in individuals infected around the time of birth and presents after prolonged latency periods ranging from 20 to 60 years. This is consistent with an age-dependent accumulation of leukemogenic events[1]. Transformed cells in ATLL are generally $CD4^+$ T lymphocytes[2], although other, less common phenotypes have been observed. These include $CD4^-CD8^-$ (refs. 3–7), $CD8^+$ (ref. 8) and $CD4^+CD8^+$ transformed cells[9,10], which suggests that infection and transformation of distinct cell populations during thymic development is important in the pathogenesis of ATLL.

The distinct clinical subtypes of ATLL include the two indolent forms, smoldering and chronic, and the extremely aggressive forms, acute and lymphomatous[2,11]. Individuals with aggressive ATLL present with extensive lymphadenopathy, hepatosplenomegaly, visceral invasion and characteristic cutaneous infiltration by malignant cells. Acute ATLL is also characterized by an aggressive high-grade T-cell leukemia, with leukemic cells showing a characteristic morphology of abnormally enlarged and cleaved nuclei, which are termed 'flower cells.' In addition to being poorly responsive to treatment, individuals with ATLL are functionally immunocompromised and develop a range of opportunistic infections similar to those seen in individuals with AIDS, such as *Pneumocystis jiroveci* pneumonia[2,11].

Although the pathogenesis of ATLL remains incompletely understood, the viral regulatory protein Tax seems to have a central role[1,12,13]. Tax, an extremely pleiotropic protein, has been shown to transform primary lymphocytes. This transformation is related to the ability of Tax to dysregulate the transcription of genes involved in cellular proliferation, cell-cycle control and apoptosis. Tax is a potent transcriptional transactivator not only of viral but also of cellular gene expression. The protein physically interacts with a number of cellular transcription factors, which include components of the NF-κB–Rel signaling complex, and persistent and constitutive activation of NF-κB is central to the development and maintenance of the malignant phenotype in ATLL[12–14]. Activation of NF-κB by Tax results in upregulation of the expression of a large number of cellular genes involved in cell proliferation, including a number of cytokines and their corresponding receptor genes[1,12–15] and this is believed to contribute to the autonomous expansion of infected and transformed cell populations.

[1]Department of Pathology, National Institute of Infectious Diseases, 4-7-1 Gakuen, Musashimurayama-shi, Tokyo 208-0011, Japan. [2]Centre for Research in Infectious Diseases, School of Medicine & Medical Science, University College Dublin, Belfield, Dublin 4, Ireland. [3]Laboratory of Molecular & Cellular Pathology and [4]Department of Molecular Pathobiology, Hokkaido University Research Center for Zoonosis Control and 21st Century COE Program for Zoonosis Control, N18 W9, Kita-ku, Sapporo, 060-8638, Japan. [5]Division of Infectious Diseases, UCLA School of Medicine, 10833 Le Conte Avenue, CHS 37-121, Los Angeles, California 90095, USA. [6]National Institute of Biomedical Innovation, Ibaraki-shi, Osaka 567-0085, Japan. [7]Department of Immunology, National Institute of Infectious Diseases, 1-23-1 Toyama, Shinjuku-ku, Tokyo 162-8640, Japan. [8]These authors contributed equally to this work. Correspondence should be addressed to W.W.H. (william.hall@ucd.ie).

Received 11 August 2005; accepted 5 December 2005; published online 19 March 2006; doi:10.1038/nm1389

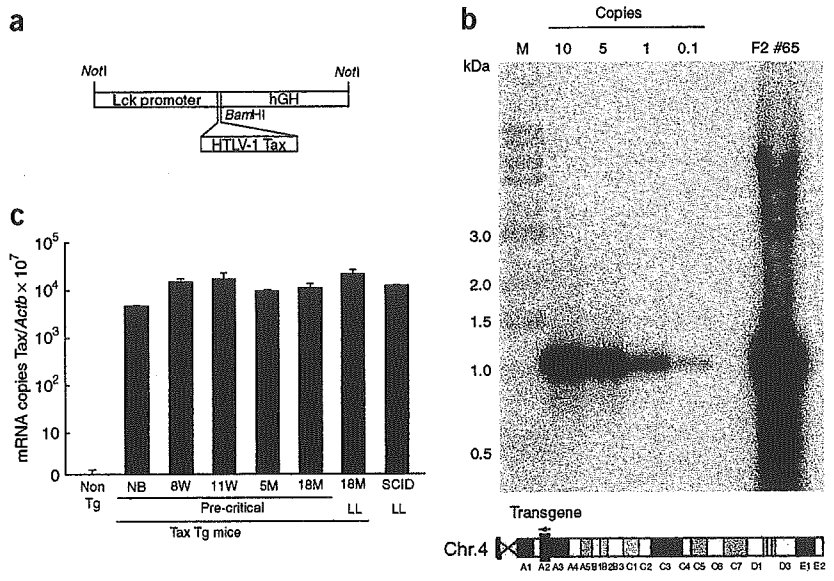

Figure 1 Construction of the Tax transgene and Tax mRNA expression in transgenic mice. (**a**) Schematic representation of the Tax transgene. HTLV-1 Tax cDNA was inserted in the *Bam*HI site of the p1017 vector at the 3′ end of the *Lck* proximal promoter. (**b**) Estimation of integrated Tax copy number and mapping of the Tax integration site (transgenic mouse #65) by chromosomal walking analysis. Tax copy numbers were investigated by Southern blot analysis of *Bam*HI-digested genomic DNA from the transgenic mouse (#65) in parallel with a serially diluted plasmid containing HTLV-I Tax cDNA. (**c**) Expression of Tax mRNA in Tax transgenic mice and SCID mice. RT-PCR was carried out on mRNAs extracted from spleens of newborn mice (NB), transgenic mice (Tg) at 8 weeks (8w), 11 weeks (11w), 5 months (5m), 18 months (18m), all without disease; 18 months with leukemia-lymphoma (18m LL) and in SCID mice with fulminant disease (SCID LL).

Attempts to directly show the oncogenic potential of Tax *in vivo* have been for the most part restricted to studies on expression of Tax in transgenic mouse models. These studies have resulted in a wide range of phenotypes, which have included the development of arthropathies, exocrinopathies, mesenchymal tumors, neurofibromas and large granular lymphocytic leukemia, a malignancy of natural killer cells[16–21]. None of the models, however, has developed T-cell lymphoma or leukemia identical to ATLL. To address this discrepancy, we have generated transgenic mice with expression of Tax restricted to developing thymocytes, and we have shown that after prolonged latency periods these mice develop lymphoma and leukemia with the clinical, pathological and immunological features characteristic of human disease.

RESULTS

Lymphoma and leukemia in HTLV-1 Tax transgenic mice

We generated transgenic mice expressing Tax under the control of the Lck proximal promoter, which restricts expression to developing thymocytes[22,23] because infection and transformation of cells during thymic development seems to be important in the pathogenesis of the disorder (**Fig. 1a**). We obtained three founder mice for each of the three lineages (#53, #14 and #17) and although each of the lineages was cross-bred with transgene-negative littermates, offspring were obtained from only one founder (#53; **Table 1**). PCR and Southern blot analysis of all founders and the progeny mice confirmed that all progeny carried the transgene. We studied transgene copy numbers and integration sites in selected mice. This number ranged from 10 to >20 copies, and genome walking analysis showed that the transgenes were tandemly inserted and integrated in the A2 region at position 14783143 of chromosome 4, which is a noncoding region (**Fig. 1b**).

Gross pathological examination of Tax founder mice #14 and #17 killed at 23 months, and of all selected offspring from founder #53 ($n = 9$) beginning at 10 months, showed the development of marked splenomegaly, hepatomegaly, lymphadenopathy and the presence of large mesenteric tumors (**Fig. 2a,b** and **Table 1**). Hepatosplenomegaly was characteristically a 5–20-fold increase in organ size (**Fig. 2a–c**). Lymphadenopathy

Table 1 Establishment of HTLV-I Tax transgenic mice

Founder	F1	F2	Gender	Killed (month)	Involvement	Leukemia
#53	#50		M	12	Liver, spleen, bone marrow	+
	#52		M	17	Liver, spleen, kidney, lymph nodes, lung, skin, bone marrow, thymus	+
		#11	M	11	Early killing	–
		#12	F	14 (dead)	Liver, spleen, kidney, lymph nodes, lung, skin	ND
		#20	F	12 (dead)	Thymus[a]	ND
		#22	F	10	Liver, spleen, kidney, lymph nodes, lung, skin, eyelid, meninges, bone marrow	+
		#33	M	10	Early killing	–
		#36	F	18	Liver, spleen, lymph nodes, lung, bone marrow, thymus	–
		#44	F	19 (dead)	Liver, spleen, lymph nodes, lung	ND
		#52	F	17	Early killing	–
		#65	M	8	Early killing	–
#14			M	23	Liver, spleen, kidney, lymph nodes, lung, skin	+
#17			F	23	Liver, spleen, kidney, lymph nodes, lung, skin	+

Offspring were generated from one of three founder mice (#53). Three mice (#11, #52, #65) were killed before the development of disease (early death). One mouse (#20) unexpectedly died. The remaining mice were killed at the time points indicated. Gross lymphomatous involvement was as noted and all tissues were subjected to histological examination. Peripheral blood smears were examined for leukemic cells using Giemsa staining. M, male; F, female; ND, not determined.
[a]Thymus was exclusively examined; other organs were not examined.

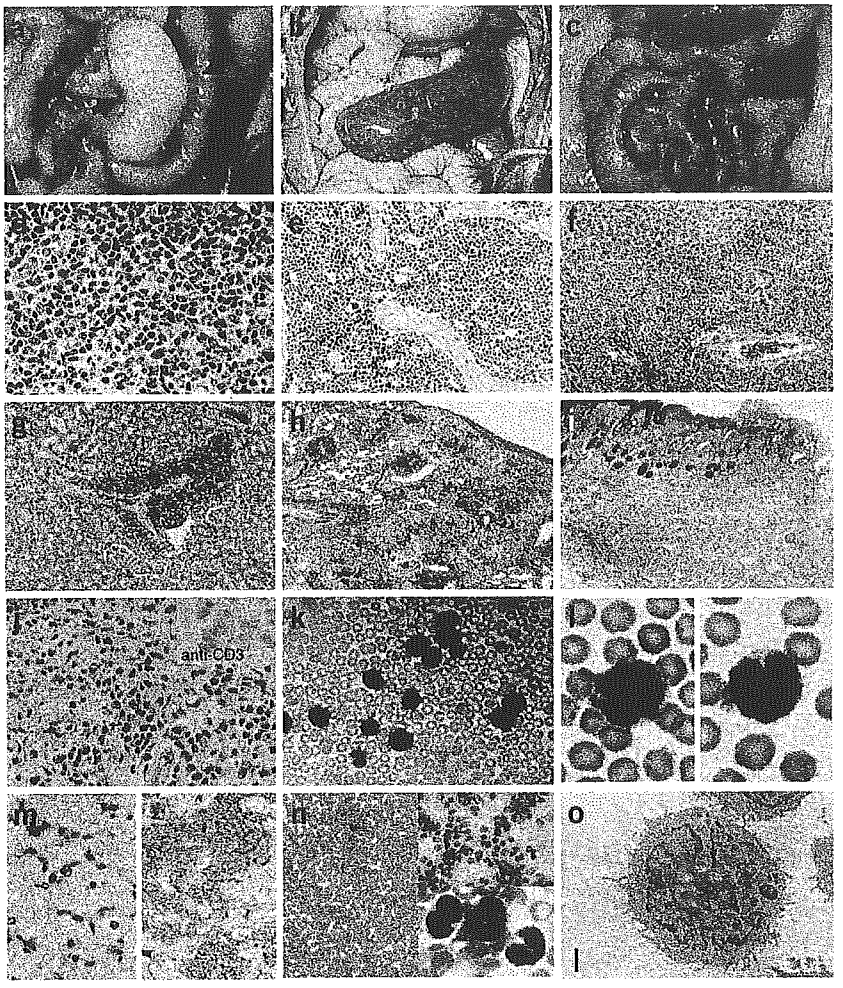

Figure 2 Pathological findings of T-cell lymphoma and leukemia in Tax transgenic mice. (**a**) Mesenteric tumor (black arrows) in the abdominal cavity of transgenic mouse #52. (**b**) Marked splenomegaly in transgenic mouse #22 with a greater than fivefold increase in size compared to an age-matched control littermate. (**c**) No tumors, lymphadenopathy or splenomegaly were evident in the control mice. Histological findings using H&E staining showed diffuse large-cell lymphoma in mesenteric lymph node (**d**), bone marrow with complete replacement of the marrow by lymphomatous cells (**e**), liver (**f**), kidney (**g**), lung (**h**) and lymphomatous infiltration of the skin with associated ulceration (**i**). (**j**) H&E staining and immunohistochemical staining with positive CD3-specific antibody staining (insert) of lymphomatous cells in the skin. (**k,l**) Peripheral blood smears from transgenic mouse #22. Leukemic cells with large and cleaved nuclei morphologically identical to flower cells found in human disease were present in peripheral blood smears of five mice. (**m**) H&E and Grocott staining of the lung showing opportunistic infection with *P. jiroveci*. (**n**) Peripheral blood smear with a large number of leukemia cells with segmented nuclei in a SCID mouse at 28 d after intraperitoneal injection of splenic lymphomatous cells from a transgenic mouse (lower magnification, left upper panel; higher magnification, left lower panel). Blood smear of a control age-matched SCID mouse is shown in the left panel. (**o**) Electron microscopic examination of leukemic cells from ascites fluid of SCID mice (original magnification, ×6,000). Cells showed enlarged cerebriform nuclei with disrupted chromatin and scanty cytoplasms typical of human ATLL cells. Scale bar, 500 nm.

was most often observed in the mesenteric, cervical and axillary lymph nodes but, in several cases, inguinal nodes were also involved. The mesenteric tumors ranged in size from 0.5 to 2.5 cm. All nine transgenic mice examined developed pathology beginning at 10 months of age, and findings were evenly distributed between males and females (**Table 1**). Histological examination showed diffuse, large-cell lymphomas involving spleen, lymph nodes, liver, thymus, bone marrow, kidney, lung, meninges and skin (**Fig. 2** and **Table 1**). Specifically, perivascular infiltration of lymphomatous cells was readily observed in the liver, kidney and lungs (**Fig. 2f–h**) and in mice with liver involvement; it seems likely that the cells had spread from the mesentery to the liver through the portal vein (**Fig. 2f**). Four mice examined had bone marrow involvement (**Fig. 2e**) with complete replacement of the marrow by lymphomatous cells. We documented involvement of the meninges in one mouse, but there was no evidence of invasion of the central nervous system parenchyma. Five of seven mice had cutaneous involvement with gross ulceration of the skin, and histologically had prominent infiltration of leukemic cells into the dermis, which is characteristic of ATLL. Immunohistochemical staining indicated that these cells expressed CD3 but not B220, showing that they were T-cell lymphomas (**Fig. 2j**). Overall, the histopathological findings are identical to those observed in ATLL, and the cytological characteristics of the lymphomatous cells are consistent with an aggressive malignancy and with the myriad of chromosomal abnormalities found in the disease[13].

Giemsa staining of peripheral blood smears in five mice showed the presence of large and abnormal leukemic cells with cleaved nuclei, which were morphologically identical to the flower cells observed in ATLL (**Fig. 2k,l**).

We also examined age- and sex-matched transgene-negative littermates in parallel for each mouse. We did not detect lymphoma in any of the nontransgenic littermates; however, two littermates that died from unknown causes did not have any abnormal gross or microscopic pathology. Three mice were killed before the development of disease, but there was no evidence of leukemia or lymphoma (**Table 1**). In addition to the development of leukemia and lymphoma, we found that transgenic mice were clinically immunocompromised. Mice with disease, but not control mice housed under identical conditions, developed severe pulmonary infections with *P. jiroveci* (**Fig. 2m**), which is characteristic of human ATLL.

Transfer of leukemia and lymphoma to immunodeficient mice

To develop a more consistent and rapid model of disease development and to facilitate immunological analyses, we attempted to induce leukemia and lymphoma in mice with severe combined immundeficiency (SCID) after intraperitoneal and intradermal injection of lymphomatous spleen cells from individual transgenic mice. After

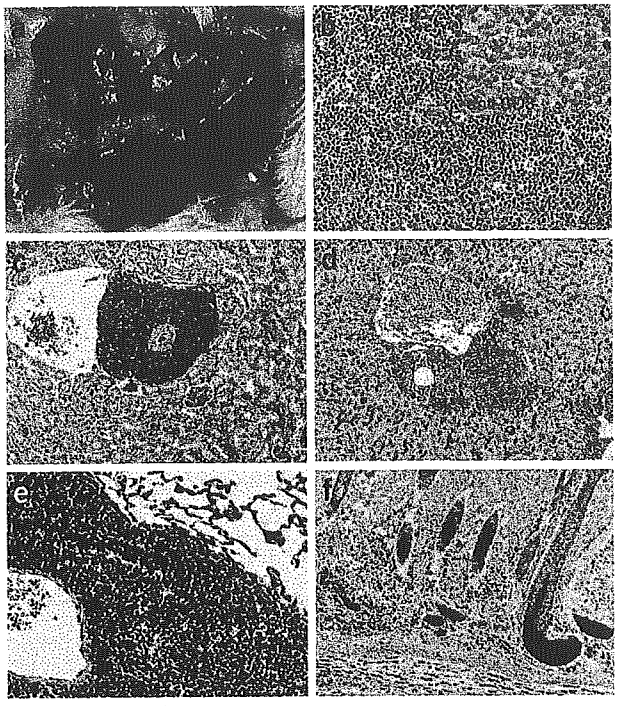

Figure 3 Gross and histological findings of lymphoma in SCID mice at 28 d after intradermal injection of lymphomatous cells from Tax transgenic mice. (**a**) Gross splenomegaly. Histological findings in spleen (**b**; insert, immunostaining showing positive staining for CD3-specific antibody), liver (**c**), kidney (**d**), lung (**e**) and skin (**f**). All organs showed extensive lymphomatous invasion.

direct transfer of cells from three transgenic mice, all SCID mice died within 28 d, having developed both an extremely aggressive leukemia with characteristic flower cells (**Fig. 2m**) and extensive lymphomatous involvement of the spleen, lymph nodes, bone marrow, liver, kidney and lung, which was identical to that observed in the original transgenic mice (**Fig. 3**). Notably, cutaneous involvement was only observed in those mice into which cells had been transferred by intradermal injection. Transmission electron microscopy of leukemic cells recovered from ascites fluid from SCID mice showed grossly enlarged and segmented cerebriform nuclei with markedly thin and scanty cytoplasms and a loss of polarity similar to that reported for ATLL and Sezary syndrome (**Fig. 2o**).

Flow cytometry analysis

We used flow cytometry to characterize the cell populations in both transgenic and SCID mice. Cells from transgenic spleens showed marked size heterogeneity with considerably higher forward scatter and side scatter compared to cells derived from spleens of control mice (**Fig. 4a**). Immunostaining of cells from SCID mice showed these were a distinct population and had a $CD3^-CD4^-CD8^-CD34^-c\text{-}kit^-$ phenotype (**Fig. 4b,c**). Staining for B-cell markers (B220) and macrophage markers (Mac 1) was negative (data not shown). Further analysis of SCID mice showed that the cells were $CD44^+CD25^+$ (**Fig. 4c**) and positive for cytoplasmic but not surface CD3 in both flow cytometric and immunofluorescence studies (**Fig. 4d,e**), all of which is consistent with a pre–T-cell, double-negative phenotype (**Fig. 4f**). A characteristic feature of ATLL is overexpression of CD25 (also known as IL-2 receptor α) on the surface of the transformed cells, and it is believed that Tax-mediated upregulation of both interleukin (IL)-2 and the IL-2 receptor has a major role in the autonomous proliferation of the transformed cell populations[14]. We examined the expression of CD25 in splenic lymphoma cells, and although the expression levels varied between tumor cells from different mice, a marked increase in expression was always evident (**Fig. 4d**). In addition, the T-cell activation marker CD69 was also found to be expressed at high levels on the lymphomatous cells (**Fig. 4d**).

NF-κB activation in transgenic and SCID mice

As it is well established that activation of NF-κB by Tax has a crucial role in transformation of cells by HTLV-I and in the maintenance of the malignant phenotype[12–14], we examined activity of NF-κB using both electrophoretic mobility shift assays (EMSAs) and enzyme-linked immunosorbent assays (ELISAs). EMSAs on nuclear extracts from transgenic splenic lymphoma cells showed marked NF-κB activity (**Fig. 5**) similar to that in a Epstein-Barr virus–transformed lymphoblastoid cell line used as a positive control. In contrast, no activity was evident in cells from normal mice (**Fig. 5a**). In addition, supershift assays (**Fig. 5b**) showed supershifted bands in the presence of antibodies for p50 and c-Rel, suggesting that formation of the p50–c-Rel complex is involved in the development and maintenance of the malignant phenotype (**Fig. 5b**). Evaluation of lymphomatous cells from SCID mice also confirmed activation of NF-κB. In contrast to the case of transgenic mice, this activation was found to involve only c-rel (**Supplementary Fig. 1** online). We also examined SCID mice by ELISA for activation of CREB, which was shown to be absent (**Supplementary Fig. 1** online).

Expression of Tax in transgenic mice

We used RT-PCR analysis of RNAs from splenic tissues to determine whether development of disease in both transgenic and SCID mice was associated with active expression of Tax (**Fig. 1c**). Although expression levels were low (10^4 less than expression of *Actb*, which encodes β-actin), Tax mRNA could be readily detected in newborn, asymptomatic, early-killed mice and in both transgenic and SCID mice with overt disease.

DISCUSSION

Here we showed that Tax expression alone in transgenic mice is sufficient to initiate the development of T-cell lymphoma and leukemia with clinical, pathological and immunological features similar or identical to those observed in ATLL. Specifically, the disorder in mice occurs after prolonged latency periods ranging from 10 to 23 months, which would be equivalent to the 20–60 years observed in human disease. The long time period before the onset of disease in the transgenic mouse model is also consistent with a multistep process of transformation. The clinical and pathological features of the disease were identical to those observed in the aggressive forms of ATLL, with widespread organ invasion by lymphomatous cells and the development of leukemia. Notably, the leukemia displayed the typical appearance of flower cells characteristic of ATLL, and these cells also had the expected morphological features when examined by electron microscopy.

ATLL has prominent cutaneous involvement, and this was reproduced in the transgenic model. Transgenic mice were also clinically immunocompromised and developed pulmonary infections with *P. jiroveci*, which is also characteristic of ATLL. The development of disease in transgenic mice and after transfer of disease to SCID mice was associated with activation of NF-κB, which is also found in ATLL.

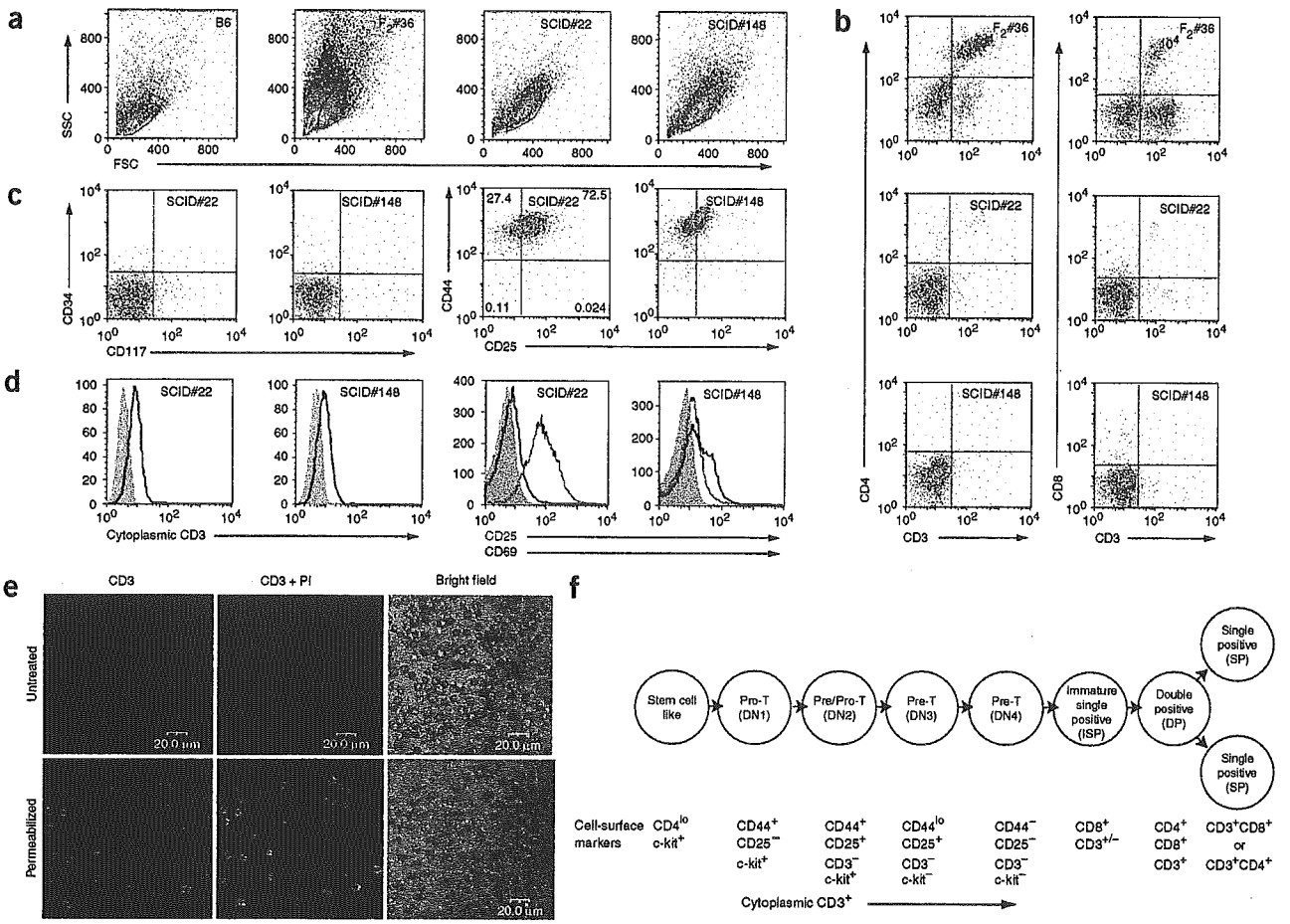

Figure 4 Flow cytometry analysis of cell-surface and intracellular markers in lymphomatous cells. We analyzed spleen-cell suspensions from transgenic mice with leukemia-lymphoma (#36), littermate control mouse (B6) and two SCID mice (#22, #148) with overt disease. (**a**) Forward-scatter (FSC) and side-scatter (SSC) analysis. (**b**) Expression of cell-surface markers CD3, CD4 and CD8. (**c**) Expression of cell-surface markers CD34, CD117 (also known as c-kit), CD44 and CD25. (**d**) Expression of CD25, CD69 and cytoplasmic CD3. (**e**) Surface and cytoplasmic CD3 staining of lymphomatous cells from SCID mice (SCID #22) with fulminant disease. Immunofluorescence studies show an absence of CD3 surface staining (untreated) but consistent and uniform cytoplasmic staining in permeabilized cells. Staining of nuclei using propidium iodide (PI) is indicated. (**f**) Schematic representation of T-cell development and corresponding immunological markers in the mouse thymus.

In the transgenic mice, this involved both the p50 and c-rel components, whereas after transfer to SCID mice, only c-rel seemed to be involved. The reasons for this are unclear, but such differences have also been observed in individuals with ATLL[24].

The malignant phenotype observed in the transgenic mice was a $CD4^-CD8^-$ double negative. Flow cytometric analysis also showed that transformed cells were $CD44^+$ and c-kit^-. Although surface staining for CD3 was negative, cytoplasmic CD3 staining was readily shown, and overall the cell markers were consistent with a thymic pre–T-cell phenotype[25,26]. The most common presenting phenotype in ATLL is $CD4^+$; however, there have been numerous reports describing the $CD4^-CD8^-$ phenotype in a considerable number of individuals with ATLL[3–7]. The different phenotypes observed in ATLL may well reflect the temporal relationships between infection with expression of Tax and the cell populations present at different stages of thymic development. It is likely that infection in most cases of human disease occurs after birth and much later than in our model. We are currently exploring the possibility of modifying the Lck promoters to allow control of Tax expression at different stages of thymic development to assess whether this will result in different phenotypes. It seems highly probable that use of the Lck promoter, which restricts expression of the transgene to developing thymocytes, has been crucial to the success of our mouse model. As noted previously, ATLL occurs after vertical transmission and is specifically associated with a history of breastfeeding. In rat models, intravenous or intraperitoneal inoculation of HTLV-I–infected cell lines results in considerable humoral and cellular immune responses. In contrast, these are absent after oral inoculation, and this hyporesponsiveness seems to contribute to successful infection[27]. Thus, both oral tolerance and the tropism of the virus for infection of developing T lymphocytes seem to be two key factors in the development of ATLL.

One major difference between our model and human disease is expression of Tax. Expression of Tax is rarely detected in ATLL, and this circumstance is thought to result primarily from highly efficient Tax-specific cellular immune responses that can effectively eliminate Tax-expressing T lymphocytes. Such responses, however, would certainly not occur in either transgenic or SCID mice. It has also been suggested that the lack of Tax expression in ATLL may be the result of

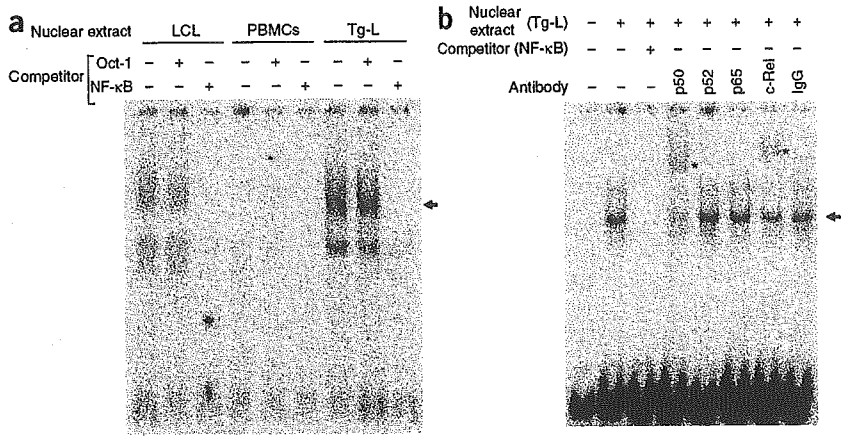

Figure 5 EMSAs showing activation of NF-κB in lymphomatous cells. (**a**) EMSAs of nuclear extracts from lymphomatous cells of transgenic mice and a positive control, the Epstein-Barr virus–transformed lymphoid cell line, and normal mouse PBMCs with a radiolabled NF-κB binding oligonucleotide probe. Specific shifted bands of NF-κB binding proteins (arrow) were exclusively detected in nuclear extracts from lymphoblastoid cell line and transgenic mice with disease (Tg-L) in the presence of the competitor. (**b**) Supershift assay of nuclear extracts from Tg-L using antibodies against p50, p65, p52, and c-Rel. Normal IgG was used as control. Supershifted bands were detected in extracts with p50-specific and c-Rel–specific antibodies.

epigenetic changes that restrict viral gene expression, but it is presently unclear whether such changes might at some point develop in this transgenic mouse model.

The models of ATLL developed in both transgenic and SCID mice will now allow detailed investigation of the role of Tax and the identification of specific molecular events associated with transformation. Moreover, the rapid development of fulminant disease in SCID mice will uniquely facilitate the evaluation of a range of therapeutic interventions that may ultimately lead to more effective treatments of human disease.

METHODS

Details are in **Supplementary Methods** online.

Mice. All mouse experimental protocols were approved by the Animal Care and Use Committee of the National Institute of Infectious Diseases, Tokyo, Japan, and by the Animal Research Ethics Committee of University College Dublin, Ireland. We purchased C57BL/6 mice from Charles River and the Oriental Yeast Company. We obtained SCID mice from Clea Japan.

Plasmid construction and generation of transgenic mice. We generated transgenic mice using inbred C57BL/6 mice and standard methods. We prepared the transgene construct (p*Lck*-Tax) by subcloning the HTLV-I Tax coding sequence into the *Bam*HI site of p1017 (provided by R.M. Perlmutter, University of Washington). We amplified Tax cDNA by PCR from DNA extracted from infected peripheral blood mononuclear cells (PBMCs). The p*Lck*-Tax plasmid was linearized by digestion with *Not*I (Boerhinger Mannheim), resulting in a 6.3-kb fragment containing the transgene, and this was purified using a Qiaex gel extraction kit (Qiagen) before injection. All mice were housed under specific pathogen-free conditions. Mice were killed after anesthesia with chloroform by syringe cardiac exsanguination. For detection of the transgene, we performed Southern blotting on genomic DNA extracted from tail-tip biopsies.

Chromosomal mapping of the inserted transgene. We identified genomic sequences flanking the transgenes by genomic walking methods[28] using the Universal Genome Walker kit (BD Bioscience Clontech) according to the manufacturer's instructions. Briefly, we constructed adaptor-ligated genomic DNA libraries of the transgenic mice using tail-tip DNA digested with four restriction enzymes: *Dra*I, *Pvu*II, *Eco*RV and *Stu*I; the genomic walk consisted of two PCR amplifications. We determined nucleotide sequences of PCR products by direct sequencing and identified specific chromosomal transgene insertion sites using BLAST searches of the flanking sequences in the Ensembl genome database.

Histopathological examination and immunohistochemistry. We directly fixed tissues in neutral-buffered formalin (Sigma), embedded them in paraffin, and sectioned and stained them with H&E. We stained additional sections with Grocott staining for detection of *P. jiroveci* cysts. We stained skin sections with CD3-specific antibody (Santa Cruz Biotechnology). We prepared peripheral blood smears using Giemsa staining and examined them with light microscopy.

Flow cytometry. We performed flow cytometry with a FACSCalibur (BD Bioscience Clontech) using standard methods. Briefly, we prepared single-cell suspensions from spleen in PBS containing 2% FCS and 0.05% sodium azide. For detection of surface antigens, we washed cells and stained them with saturating amounts of antibodies conjugated with FITC, PE or APC in the presence of blocking antibody 2.4G2 (FcR-specific) monoclonal antibody for 20 min on ice. For analysis of live cells, we added propidium iodide at a final concentration of 5 μg/ml. For detection of intracellular CD3, we stained cells with ethidium monoazide bromide (5 μg/ml), fixed them with 4% formaldehyde in PBS and incubated them in permeabilization buffer containing 0.5% saponin. We incubated cells with FITC-conjugated CD3-specific antibody or control monoclonal antibody (rat IgG2b). We carried out analysis using the Cell Quest program and reanalyzed data using FlowJo software (Tree Star) by gating live cells. Specific monoclonal antibodies used are detailed in **Supplementary Methods** online.

Immunofluorescence studies of surface and cytoplasmic CD3 staining. We collected cells (10^6) directly from spleen tissues from SCID mice, and washed and incubated them with CD3-specific antibody. Thereafter, we incubated samples with Alexa 488R–conjugated goat rabbit-specific IgG and then stained with propidium iodide (1 μg/ml). We permeabilized cells before incubation with primary antibody and detected immunofluorescent signals using a confocal microscope (IX70, Olympus).

EMSAs. We prepared nuclear extracts from 1–10 × 10^6 of lymphomatous cells from spleens of transgenic mice, an Epstein-Barr virus–transformed lymphoblastoid cell line, and PBMCs from control mice as previously described[29]. We performed an EMSA with the Gel Shift Assay Systems kit (Promega) according to the manufacturer's protocol. We separated samples by electrophoresis on 4% polyacrylamide gels in 0.25% Tris–boric acid–EDTA, and dried and analyzed them using a BAS 2000 image analyzer (Fujifilm).

Real-time quantitative PCR. We used real-time PCR (RT-PCR) to quantify expression of Tax mRNA in transgenic and SCID mice. We harvested spleens at birth and at 8 weeks, 11 weeks, 5 months, 18 months in transgenic mice without disease, and at 18 months in mice with leukemia-lymphoma, from control littermates and from SCID mice after intraperitoneal transfer of lymphomatous cells. We measured levels of Tax mRNA by RT-PCR after reverse transcription using the ABI PRISM 7900 sequence detection system (Applied Biosystems) with a QuantiTect Probe PCR kit (Qiagen).

Transfer of leukemia and lymphoma to SCID mice. We harvested spleen cells from transgenic mice and directly suspended them in RPMI medium. We directly injected cells (10^6) intraperitoneally or intradermally into SCID mice

from three individual transgenic animals. At 28 d, when mice were clearly ill, we carried out pathological and immunological studies as above.

Electron microscopy. We collected cells from ascites of SCID mice and fixed them in 2.5% glutaraldehye and 2% paraformaldehyde, postfixed them in 1% osmium tetroxide, dehydrated them and embedded them in epoxy resin. We stained ultrathin, 80-nm sections with uranyl and lead acetate and examined them with a JEM-1220 electron microscope (Jeol Datum) at 80 kV.

URL. Ensembl, http://www.ensembl.org

Note: Supplementary information is available on the Nature Medicine website.

ACKNOWLEDGMENTS

We thank Y. Sato and E. Tao for their technical assistance. We also thank O. Suzuki, T. Suzuki, M. Moriyama, K. Iwabuchi and Y. Misaki for advice. Y.O. is a Research Fellow of the Japanese Society for the Promotion of Science. These studies were supported by the Japanese Foundation for AIDS Prevention, Core Research for Evolutional Science and Technology (CREST), Ministry of Education and Culture, Japan and the National Virus Reference Laboratory, University College Dublin, Ireland.

COMPETING INTERESTS STATEMENT

The authors declare that they have no competing financial interests.

Published online at http://www.nature.com/naturemedicine/
Reprints and permissions information is available online at http://npg.nature.com/reprintsandpermissions/

1. Matsuoka, M. Human T-cell leukemia virus type I and adult T-cell leukemia. *Oncogene* **22**, 5131–5140 (2003).
2. Takatsuki, K. *et al.* Clinical diversity in adult T-cell leukemia-lymphoma. *Cancer Res.* **45**, 4644s–4645s (1985).
3. Hattori, T. *et al.* Leukaemia of novel gastrointestinal T-lymphocyte population infected with HTLV-I. *Lancet* **337**, 76–77 (1991).
4. Suzushima, H. *et al.* Double-negative (CD4- CD8-) T cells from adult T-cell leukemia patients also have poor expression of the T-cell receptor alpha beta/CD3 complex. *Blood* **81**, 1032–1039 (1993).
5. Kamihira, S. *et al.* Unusual morphological features of adult T-cell leukemia cells with aberrant immunophenotype. *Leuk. Lymphoma* **12**, 123–130 (1993).
6. Suzushima, H., Asou, N., Hattori, T. & Takatsuki, K. Adult T-cell leukemia derived from S100 beta positive double-negative (CD4- CD8-) T cells. *Leuk. Lymphoma* **13**, 257–262 (1994).
7. Shimauchi, T., Hirokawa, Y. & Tokura, Y. Purpuric adult T-cell leukaemia/lymphoma: expansion of unusual CD4/CD8 double-negative malignant T cells expressing CCR4 but bearing the cytotoxic molecule granzyme B. *Br. J. Dermatol.* **152**, 350–352 (2005).
8. Yamada, Y. *et al.* Adult T-cell leukemia with atypical surface phenotypes: clinical correlation. *J. Clin. Oncol.* **3**, 782–788 (1985).
9. Ohata, J. *et al.* CD4/CD8 double-positive adult T-cell leukemia with preceding cytomegaloviral gastroenterocolitis. *Int. J. Hematol.* **69**, 92–95 (1999).
10. Ciminale, V. *et al.* Unusual CD4+CD8+ phenotype in a Greek patient diagnosed with adult T-cell leukemia positive for human T-cell leukemia virus type I (HTLV-I). *Leuk. Res.* **24**, 353–358 (2000).
11. Uchiyama, T., Yodoi, J., Sagawa, K., Takatsuki, K. & Uchino, H. Adult T-cell leukemia: clinical and hematologic features of 16 cases. *Blood* **50**, 481–492 (1977).
12. Yoshida, M. Multiple viral strategies of HTLV-1 for dysregulation of cell growth control. *Annu. Rev. Immunol.* **19**, 475–496 (2001).
13. Jeang, K.T., Giam, C.Z., Majone, F. & Aboud, M. Life, death, and tax: role of HTLV-I oncoprotein in genetic instability and cellular transformation. *J. Biol. Chem.* **279**, 31991–31994 (2004).
14. Sun, S.C. & Yamaoka, S. Activation of NF-kappaB by HTLV-I and implications for cell transformation. *Oncogene* **24**, 5952–5964 (2005).
15. Hall, W.W. & Fujisawa, M. Deregulation of cell-signalling pathways in HTLV-I infection. *Oncogene* **24**, 5965–5975 (2005).
16. Nerenberg, M., Hinrichs, S.H., Reynolds, R.K., Khoury, G. & Jay, G. The tat gene of human T-lymphotropic virus type 1 induces mesenchymal tumors in transgenic mice. *Science* **237**, 1324–1329 (1987).
17. Hinrichs, S.H., Nerenberg, M., Reynolds, R.K., Khoury, G. & Jay, G. A transgenic mouse model for human neurofibromatosis. *Science* **237**, 1340–1343 (1987).
18. Green, J.E., Hinrichs, S.H., Vogel, J. & Jay, G. Exocrinopathy resembling Sjogren's syndrome in HTLV-1 tax transgenic mice. *Nature* **341**, 72–74 (1989).
19. Iwakura, Y. *et al.* Induction of inflammatory arthropathy resembling rheumatoid arthritis in mice transgenic for HTLV-I. *Science* **253**, 1026–1028 (1991).
20. Green, J.E., Baird, A.M., Hinrichs, S.H., Klintworth, G.K. & Jay, G. Adrenal medullary tumors and iris proliferation in a transgenic mouse model of neurofibromatosis. *Am. J. Pathol.* **140**, 1401–1410 (1992).
21. Grossman, W.J. *et al.* Development of leukemia in mice transgenic for the tax gene of human T-cell leukemia virus type I. *Proc. Natl. Acad. Sci. USA* **92**, 1057–1061 (1995).
22. Chaffin, K.E. *et al.* Dissection of thymocyte signaling pathways by *in vivo* expression of pertussis toxin ADP-ribosyltransferase. *EMBO J.* **9**, 3821–3829 (1990).
23. Wildin, R.S. *et al.* Developmental regulation of lck gene expression in T lymphocytes. *J. Exp. Med.* **173**, 383–393 (1991).
24. Mori, N. *et al.* Constitutive activation of NF-kappaB in primary adult T-cell leukemia cells. *Blood* **93**, 2360–2368 (1999).
25. Staal, F.J., Weerkamp, F., Langerak, A.W., Hendriks, R.W. & Clevers, H.C. Transcriptional control of T lymphocyte differentiation. *Stem Cells* **19**, 165–179 (2001).
26. Rezuke, W.N., Abernathy, E.C. & Tsongalis, G.J. Molecular diagnosis of B- and T-cell lymphomas: fundamental principles and clinical applications. *Clin. Chem.* **43**, 1814–1823 (1997).
27. Kannagi, M., Ohashi, T., Harashima, N., Hanabuchi, S. & Hasegawa, A. Immunological risks of adult T-cell leukemia at primary HTLV-I infection. *Trends Microbiol.* **12**, 346–352 (2004).
28. Noguchi, A. *et al.* Chromosomal mapping and zygosity check of transgenes based on flanking genome sequences determined by genomic walking. *Exp. Anim.* **53**, 103–111 (2004).
29. Dignam, J.D., Martin, P.L., Shastry, B.S. & Roeder, R.G. Eukaryotic gene transcription with purified components. *Methods Enzymol.* **101**, 582–598 (1983).

Available online at www.sciencedirect.com
SCIENCE DIRECT®
Theriogenology
ELSEVIER
Theriogenology 64 (2005) 112–122
www.journals.elsevierhealth.com/periodicals/the

Sensitivity to chilling of medaka (*Oryzias latipes*) embryos at various developmental stages

Delgado M. Valdez Jr., Akira Miyamoto, Takao Hara, Keisuke Edashige, Magosaburo Kasai*

Laboratory of Animal Science, College of Agriculture, Kochi University, Nankoku, Kochi 783-8502, Japan

Received 15 July 2004

Abstract

As an essential step toward cryopreservation of fish embryos, we examined the chilling sensitivity of medaka (*Oryzias latipes*) embryos at various developmental stages. Embryos at the 2–4 cell, 8–16 cell, morula, blastula, and early gastrula stages were suspended in Hanks solution. They were chilled to various temperatures (usually 0 °C), kept for various periods (usually 20 min), then cultured for up to 14 d to determine survival (assessed by the ability to hatch). Embryos at the 2–4 cell stage were the most sensitive to chilling to 0 °C, but sensitivity decreased as development proceeded. The survival rate of 2–4 cell embryos was affected after 2 min of chilling at 0 °C; although the rate decreased gradually as the duration of chilling increased, 38% of them still survived after 40 min of chilling. Embryos at the 2–4 cell stage were sensitive to chilling at 0 or −5 °C, but much less sensitive at 5 or 10 °C. The survival rate of 2–4 cell embryos subjected to repeated rapid cooling and warming was similar to that of those kept chilled. When early gastrula embryos were preserved at 0 or 5 °C, the hatching rate did not decrease after 12 and 24 h of chilling, respectively, but then decreased gradually as storage was prolonged; however, 3–10% of the embryos hatched even after storage for 10 d. In conclusion, although later-stage medaka embryos would be suitable for cryopreservation (from the perspective of chilling sensitivity), chilling injury may not be serious in earlier stage embryos.

Keywords: Medaka; Embryo; Chilling injury; Refrigeration; Developmental stage

* Corresponding author. Tel.: +81 88 864 5194; fax: +81 88 864 5219.
E-mail address: mkasai@cc.kochi-u.ac.jp (M. Kasai).

0093-691X/$ – see front matter © 2004 Elsevier Inc. All rights reserved.
doi:10.1016/j.theriogenology.2004.11.006